Modern Physics Letters B
(2023) 2250213 (15 pages)

DOI: 10.1142/S021798492250213X

Exploration of thermal conductivity and optical properties of β- and γ-nitrogene

Baowei Cao*, Huimin Zhuang†, Xiaoying Wang‡, Minxuan Feng‡, Yingchun Ding†,§,‖ and Zhibin Gao‡,¶,‖

*School of Chemistry and Chemical Engineering, Yulin University, Yulin, 719000, P. R. China

†College of Optoelectronics Engineering, Chengdu University of Information Technology, Chengdu 610225, P. R. China

‡State Key Laboratory for Mechanical Behavior of Materials, Xi'an Jiaotong University, Xi'an 710049, P. R. China

§dyccqzx@cuit.edu.cn

¶zhibin.gao@xjtu.edu.cn

Received 19 July 2022
Revised 11 October 2022
Accepted 8 December 2022
Published 2 February 2023

In this paper, the thermal conductivity and optical properties of β- and γ-nitrogene have been investigated by the first principles of density functional theory. Phonon dispersion suggests that β- and γ-nitrogene are stable. The thermal conductivity of β-nitrogene is almost isotropic and has a thermal conductivity of 960.17 W/m · K at 300 K. The thermal conductivity of γ-nitrogene is anisotropic, which has a thermal conductivity of 12.34 W/m · K and 18.59 W/m · K along with the armchair and zigzag directions at 300 K, respectively. The acoustic phonon branches (TA, LA, and ZA) play a dominant role in heat transport in β-nitrogene. But optical dispersions play an important role in the heat transport of γ-nitrogene. With the larger Grüneisen parameter and smaller phonon lifetime of γ-nitrogene, γ-nitrogene exhibits a smaller thermal conductivity than that of β-nitrogene significantly. In addition, optical properties of β- and γ-nitrogene have been researched. Meanwhile, γ-nitrogene has a certain absorption effect on the visible spectrum and ultraviolet light. Thus, the nitrogene allotropes have different optoelectronic properties. Moreover, nitrogene can be used to fabricate optoelectronic devices. This work provides a theoretical description of the thermal conductivity and photoelectricity of nitrogene allotropes.

Keywords: Nitrogene; first-principles; thermal conductivity; optical properties.

PACS Number(s): 61.50.Ks, 71.20.Ps, 62.50.+p

‖Corresponding authors.

1. Introduction

In recent years, two-dimensional (2D) materials are the focus of scientific research due to their ascendant characteristics and latent applications. New 2D materials have brought a new field of research to experiment and theory. 2D group-V materials such as nitrogene,[1] phosphorene,[2] arsenene,[3] antimonene,[4,5] and bismuthene[6] have attracted much attention due to their excellent physical properties. Thus, the research of 2D materials in group V has become one of the interesting topics recently.[7–10] For instance, Liu *et al.*[11] reported that phosphorene was a semiconductor with desirable hole mobility, which can construct a 2D CMOS inverter consisting of phosphorene PMOS. It has been pointed out that arsenene and antimonene are wide-band gap semiconductors with high stability.[12,13]

2D Group-V materials (nitrogene, phosphorene, arsenene, antimonene, and bismuthene) have some allotropes[1–29] with the same main group in the periodic table. Nitrogene has been found two different structures of the monolayer honeycomb, i.e. nitrogene and octagon–nitrogene.[10–16] Subsequently, the existence and gap engineering of nitrogene have been investigated theoretically.[17,18] Peng *et al.*[19] studied the thermal conductivity of buckled hexagonal structures of monatomic 2D materials. In these single-layer buckled honeycomb structure 2D materials of the group-V monolayer, the blue nitrogene (β-nitrogene) has the largest thermal conductivity with 763.4 W/m K except graphene (3716.6 W/m K) at 300 K.[19]

The anisotropic thermal conductivity of armchair and zigzag directions in 2D Group-V elements (phosphorene,[20–24] antimonene,[20,25,26] arsenene[20,27,28] and bismuthene[29]) have been researched. In phosphorene, the thermal conductivities have been calculated to be 13 W/m $\cdot$ K and 30 W/m $\cdot$ K along the armchair and zigzag directions, respectively.[22] The thermal conductivities are on par with those found in traditional bulk thermoelectric materials (typically < 5 W/m $\cdot$ K).[23,24] Antimonene has a low lattice thermal conductivity (15.1 W/m $\cdot$ K at 300 K).[26] The low thermal conductivity of a few different arsenene structures, i.e., buckled, puckered, and square, and room temperature values ranges from 2.5 W/m $\cdot$ K to 7 W/m $\cdot$ K.[20,27,28] First-principles calculations show that the lowest lattice thermal conductivity is orthogonal to each other in phosphorene[24] and arsenene,[28] thereby enhancing the ratio between the two values and maximizing the ZT. Theoretical studies predict high ZT values approaching 2.1 at 300 K (Ref. 25) in buckled antimonene and 2.1 and 2.4 at 300 K (Ref. 29) for n- and p-doped bismuthene, respectively.

Here, we have predicted four different structures of monolayer that consist of nitrogen atoms: honeycomb nitrogene (β-nitrogene) and other nitrogene (α-, γ- and δ-nitrogene). Up to now, the phonon transport and photoelectric properties of nitrogene allotropes are far from clear. In this paper, for the first time, the electronic structure and optical properties of nitrogene allotropes have been investigated, including the calculated phonon dispersion, thermal conductivity, band

structure, and optical properties. The stability of nitrogene allotropes (β- and γ-nitrogene) is further verified by phonon dispersion. These findings indicate that β- and γ-nitrogene monolayers may be promising materials in electronic devices.

2. Calculation Models and Methods

The supercells ($3 \times 3 \times 1$) of β- and γ-nitrogene are shown in Fig. 1. In the direction perpendicular to the nitrogene plane, the vacuum region of 20 Å is imposed to ensure that the neighboring supercells do not interact with each other. The lattice thermal conductivity and optical properties of monolayer nitrogene allotropes have been calculated using Vienna *Ab initio* Simulation Package (VASP).[30] We choose the generalized gradient approximation (GGA) in the Perdew–Burke–Ernzerhof (PBE) parametrization for the exchange-correlation functional.[31,32] PAW-PBE method has been indicated to be a very effective calculation for 2D materials.[33–35]

The PHONOPY code[36] was used to calculate the phonon spectrum of four nitrogene allotropes at the level of harmonic approximation. In the approach to obtain lattice thermal conductivity, the second-order inter-atomic forces constants (IFCs) were computed by the finite difference method. All third-order IFCs were extracted from second-order IFCs using a real-space finite difference method as implemented in the ShengBTE code.[37–39] The cutoff energy for the plane-wave basis

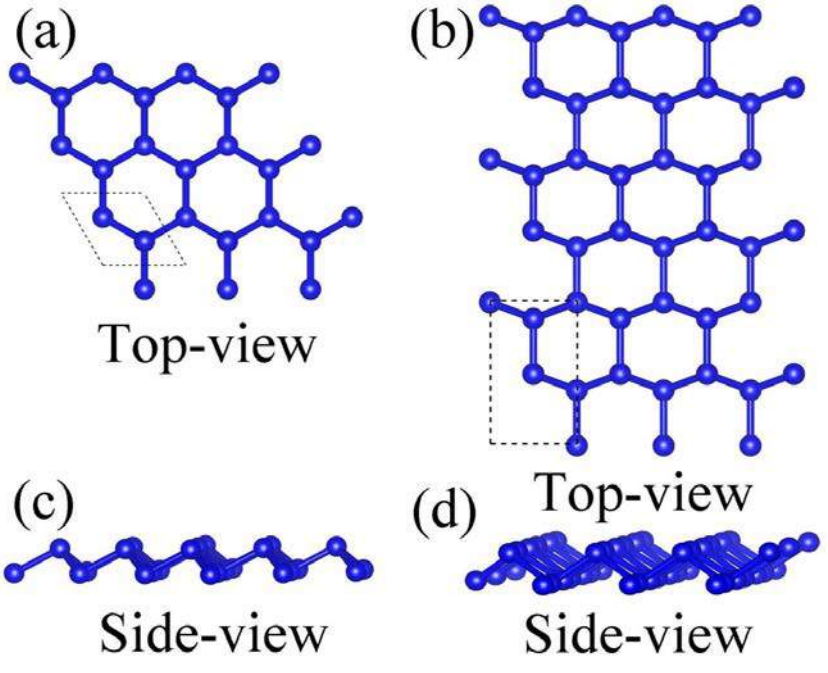

Fig. 1. (Color online) The supercells ($3 \times 3 \times 1$) of β-nitrogene (a) and γ-nitrogene (b).

set is 500 eV. The Brillouin zones are sampled with a $9 \times 9 \times 1$ k-points grid. All atoms were fully relaxed until the convergence tolerance of the total energy from the last two sequential steps is less than 10^{-4} eV/atom, as well as the maximum force on each atom, is less than 10^{-4} eV/Å.

3. Results and Discussion

3.1. *Phonon dispersion*

Figure 1 shows the geometric structure of β- and γ-nitrogene (α- and δ-nitrogene are shown in Fig. S1). Each primitive cell contains two and four nitrogen atoms of β- and γ-nitrogene, respectively (see Supporting information materials). In supercell structures, a new structure of γ-nitrogene has a buckling structure similar to β-nitrogene. The stable geometric structure of β-nitrogene has been obtained by performing structure optimization in previous work.[19,20] While in this paper, in order to investigate the stability of β- and γ-nitrogene, the phonon dispersion has been calculated. For β- and γ-nitrogene, the phonon dispersion is shown in Fig. 2. In Fig. 2, we show the obtained phonon spectrums of β- and γ-nitrogene along the path Γ (0 0 0)–M (0 0.5 0)–K (1/3 2/3 0)–Γ (0 0 0) and Γ (0 0 0)–X (0.2534 0.2534 0)–S (0 1/2 0)–Y (−1/2 1/2 0)–Γ (0 0 0) in the first Brillouin zone, respectively. As shown in Fig. 2, the imaginary frequency of vibration modes is not found for the whole Brillouin zone, which indicates that β- and γ-nitrogene are dynamically stable. But α- and δ-nitrogene are dynamically unstable (see Fig. S2).

In Fig. 2, the calculated phonon dispersion reveals that in addition to the two acoustic branches with linear dispersion for the in-plane modes (longitudinal acoustic and transverse acoustic modes, LA and TA), both nitrogene allotropes have the third out-of-plane branch (flexural acoustic mode, ZA) with a quadratic dispersion, which is a typical signature of 2D materials.[19,31] The largest frequency in the phonon dispersion is 32.5 THz and 29 THz for β- and γ-nitrogene, respectively,

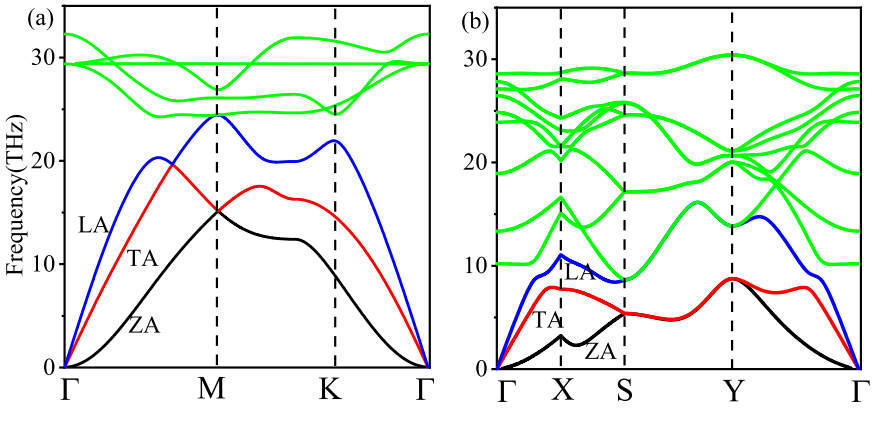

Fig. 2. (Color online) Phonon dispersion curves for (a) β-nitrogene and (b) γ-nitrogene.

which is significantly lower than that of graphene (around 48 THz),[19] and slightly lower than that of 34 THz and 38 THz for β_{12} and χ_3 borophene.[31]

These acoustic modes play an important role in the phonon transport properties of materials. The lowest frequency acoustic mode (ZA) of β-nitrogene is 15 HTz, which is three times as large as that of γ-nitrogene in the phonon dispersion. For β-nitrogene, the frequency of acoustic modes (LA and TA) is larger than that of γ-nitrogene.

3.2. *Lattice transport properties*

The thermal conductivity has been predicted between 100 K and 800 K for β- and γ-nitrogene in Fig. 3. In the classic phonon transport theory, the relaxation time due to the U-scattering process is inversely proportional to the phonon population as in the high-temperature limit. As can be seen from Fig. 3, the lattice conductivities of β- and γ-nitrogene decrease with the increase in temperature, following the universal relation. The thermal conductivity of β-nitrogene is almost isotropic, which is 960.17 W/m · K (Fig. 3(a)) at 300 K. But the thermal conductivity of γ-nitrogene is anisotropic, which has the thermal conductivity of 12.34 W/m · K and 18.59 W/m · K along with the armchair and zigzag directions (Fig. 3(b)) at room temperature, respectively.

For γ-nitrogene, the obtained lattice conductivity (zigzag direction) is slightly larger than that of armchair direction except for 100 K. Peng *et al.*[19] reported that the thermal conductivity of β-nitrogene was 763.4 W/m K at 300 K. Our value is larger than the calculated result by Peng *et al.* at the same temperature.[19] These results show that the lattice thermal conductivity of β-nitrogene is similar in magnitude to that of hydrogenated graphene (876 W/m K) and hexagonal boron nitride (600 W/m · K).[19] But the lattice thermal conductivity of γ-nitrogene is larger than that of phosphorene (5 W/m K),[23,24] antimonene (7.9 W/m K) and arsenene (7 W/m · K).[19,20,27,28]

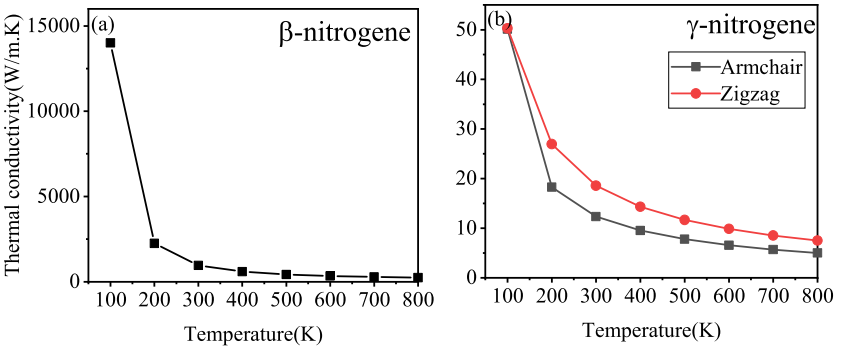

Fig. 3. (Color online) The calculated lattice thermal conductivities of β-nitrogene (a) and γ-nitrogene (b) as a function of temperature.

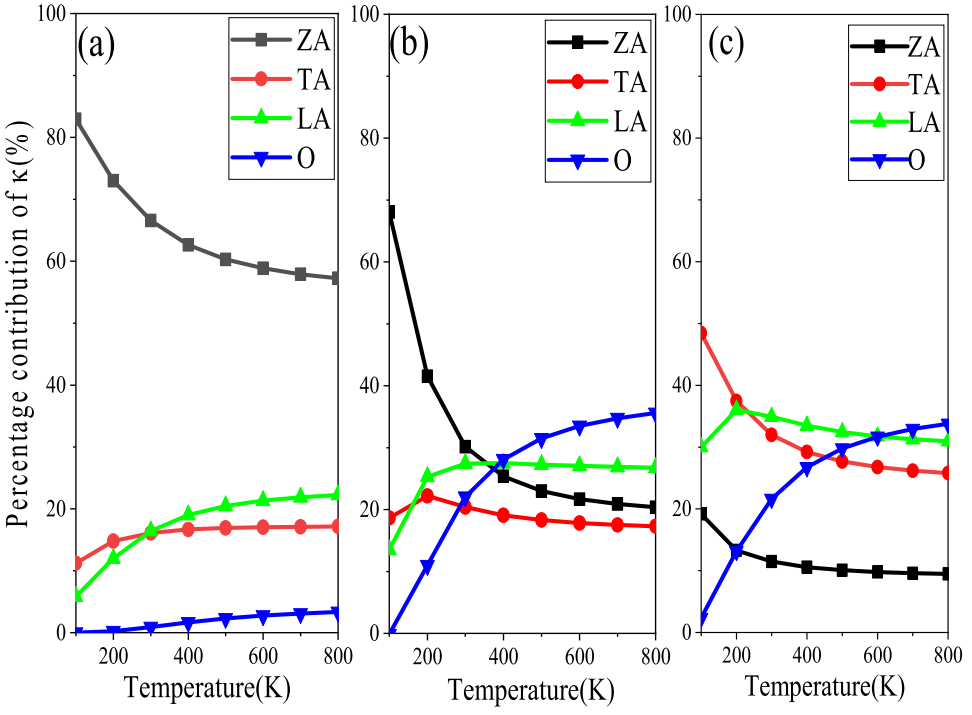

Fig. 4. (Color online) Percentage contribution (β-nitrogene (a) and γ-nitrogene (b) and (c)) of each phonon branch to total K in different directions as a function of temperature.Percentage contribution along the armchair (b) and zigzag (c) of γ-nitrogene.

In Fig. 4, we show the calculated percentages of thermal conductivity for β-nitrogene (Fig. 4(a)) and γ-nitrogene (Figs. 4(b) and 4(c)) to the corresponding total values, dissociated into each phonon branch. The thermal conductivity of the monolayer is mainly attributed to three acoustic branches, LA, TA, and ZA. For percentages of thermal conductivity of β-nitrogene are shown in Fig. 4(a). Among them, optical dispersion plays a minor role in monolayer heat transport. The total contribution to thermal conductivity is roughly 4% at 800 K. On the other hand, three acoustic branches still play the dominant role in the thermal conductivity of β-nitrogene. It is also interesting that the heat transfer of the monolayer is mainly conducted through the ZA phonon branch, which is about 57% at 800 K. The percentages of thermal conductivity in acoustic phonon branches (TA and LA) are about 17% and 22% at 800 K, respectively.

But for γ-nitrogene (Figs. 4(b) and 4(c)), the optical dispersions play an important role in monolayer heat transport, which is roughly 36% and 34% above 400 K. For γ-nitrogene, these results have indicated that the optical phonon plays a more significant role in thermal conduction of monolayer than acoustic branches, which is obviously in contrast to that of β-nitrogene.

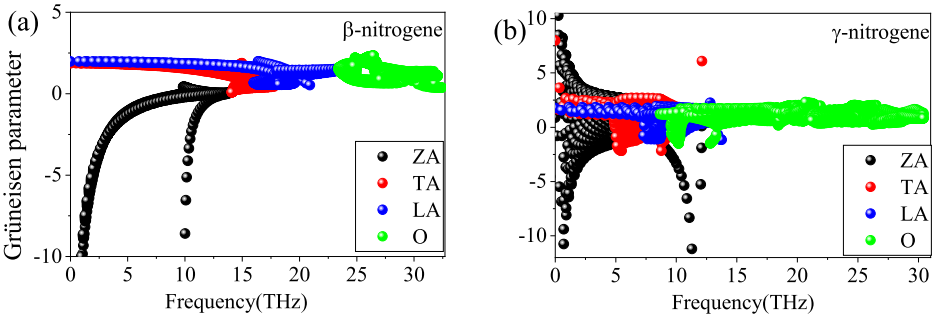

Fig. 5. (Color online) The mode Grüneisen parameter of β-nitrogene (a) and γ-nitrogene (b).

The mode-Grüneisen parameter ($\gamma(\omega)$) provides information about anharmonic interactions, and a larger mode-Grüneisen parameter ($\gamma(\omega)$) implies strong anharmonicity, leading to low lattice thermal conductivity. To gain a better understanding of the thermal transport properties of β- and γ-nitrogene, we have researched the phonon scattering processes as a function of frequency at 300 K in terms of mode-Grüneisen parameter, phonon relaxation time, and scattering channels in phase space in detail. First, the calculated mode-Grüneisen parameters are displayed in Fig. 5. It was computed by

$$\gamma(\omega) = -\frac{V_0}{\omega_j(q)}\frac{\partial\omega_j(q)}{\partial V_0}, \tag{1}$$

where V_0 is the equilibrium volume, j is the phonon branch index, and $\mathbf{q}$ is the wave vector. From Fig. 5(a), the acoustic branches (TA and LA) and the optical phonon modes (O) also have smaller $\gamma(\omega)$ values than that of the acoustic branches (ZA). This smaller $\gamma(\omega)$ implies slight anharmonicity, leading to high lattice thermal conductivity. In Fig. 5(b), the acoustic branches (ZA, TA, and LA) and the optical phonon modes (O) give large values $\gamma(\omega)$ of γ-nitrogene, leading to low lattice thermal conductivity.

In Figs. 5(a) and 5(b), many phonon modes in the ZA branch exhibit the largest negative mode-Grüneisen parameters. The phonon-mode averaged Grüneisen constants of β- and γ-nitrogene are found to be -0.22 and 1.06, respectively. In the semi-empirical theory,[6,46] the relaxation time of phonon–phonon Umklapp scattering is inversely proportional to $\gamma(\omega)^2$. Therefore, the heat transfer is suppressed for the phonon modes with large Grüneisen parameters. The value of the Grüneisen parameter ($\gamma(\omega)$) in γ-nitrogene is a bit larger than that of β-nitrogene, especially in respect of the $\gamma(\omega)$ about three acoustic phonon branches. The larger Grüneisen parameter ($\gamma(\omega)$) indicates stronger phonon anharmonicity in γ-nitrogene, resulting in stronger phonon–phonon scattering. As a result, stronger phonon–phonon scattering leads to a smaller phonon lifetime of γ-nitrogene.

In Fig. 6, we show the calculated total relaxation times (τ). One should note that the relaxation time of a phonon mode is related to its scattering rate by the

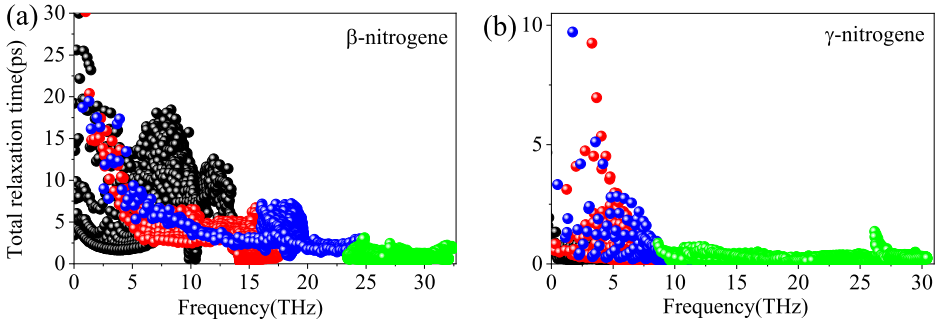

Fig. 6. (Color online) The total relaxation time of each phonon branch of β-nitrogene (a) and γ-nitrogene (b) as a function of frequency.

relation $\Omega(q,\omega) = 1/\tau(q,\omega)$, which Ω represents the phonon scattering rate. It is worth mentioning that the three-phonon Umklapp scattering, which gives a $1/T$ relationship, is expected to be the dominant mechanism in the three-phonon scattering process at a very high temperature. From Figs. 6(a) (β-nitrogene) and 6(b) (γ-nitrogene), we can see that all-optical phonon (O) modes show smaller relaxation times, compared to that low-frequency acoustic (A) phonons. The average relaxation time of optical (O) modes is roughly 2 ps (β-nitrogene) and 1 ps (γ-nitrogene), which are in contrast to 10 ps (β-nitrogene) and 2.5 ps (γ-nitrogene) in the case of acoustic (A) modes. Therefore, for three-phonon processes (U- and N-processes), the average scattering rate of optical (O) modes is approximately 5 and 2.5 times larger than those of acoustic (A) modes.

We find the reasons for the significant contribution from acoustic (A) and optical (O) branches to the total thermal conductivity of β- and γ-nitrogene. In Eqs. (2) and (3), the frequency-dependent group velocities (v_{g}) and phonon relaxation time (τ) of each phonon branch for the two materials are given according to the definition of thermal conductivity (κ):

$$\kappa = C_V vl/3 = C_V v_g^2 \tau/3. \tag{2}$$

The frequency-dependent group velocities (v_{g}):

$$v = \frac{\partial \omega}{\partial q}. \tag{3}$$

In Figs. 6(a) and 6(b), the group velocities (v_{g}) have been researched according to phonon dispersion curves of β- and γ-nitrogene from Figs. 2(a) and 2(b). These results have shown that the group velocities (v_{g}) of β-nitrogene are significantly larger than that of γ-nitrogene. From Figs. 6(a) and 6(b), the phonon relaxation time (τ) of β-nitrogene is also larger than that of γ-nitrogene. From these results, the thermal conductivity (κ) of β-nitrogene is significantly larger than that of γ-nitrogene in Figs. 3(a) and 3(b).

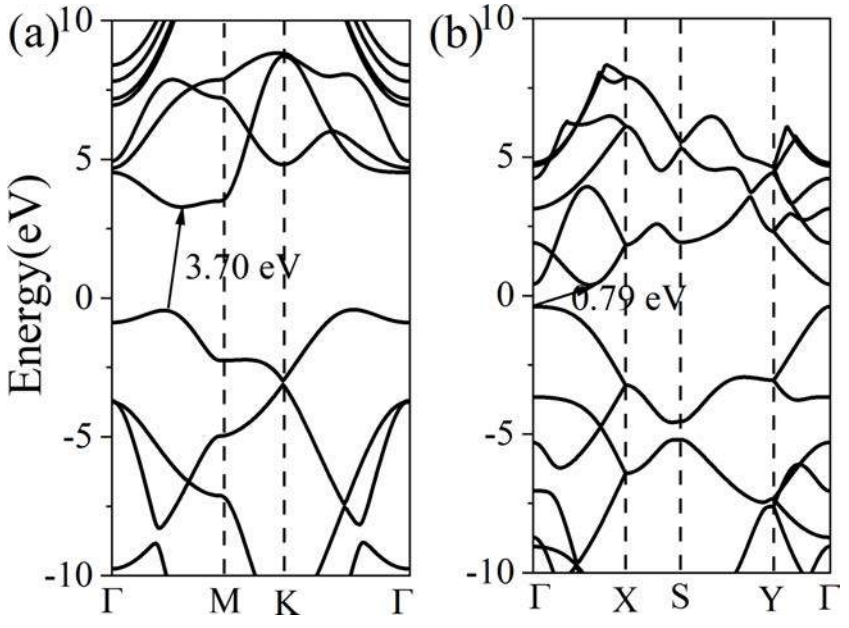

Fig. 7. (Color online) Band structures for (a) β-nitrogene and (b) γ-nitrogene.

3.3. *Energy band structures*

The band structures of β- and γ-nitrogene are described in Fig 7. It is demonstrated that the β- and γ-nitrogene are semiconductors with band energy gaps (Eg) of 3.70 eV and 0.79 eV. The results show that β- and γ-nitrogene have an indirect band energy gap (Eg), which means that β- and γ-nitrogene are also indirect gap semiconductors. The band gap (Eg) with 3.70 eV for β-nitrogene is in an excellent agreement with the previous report results of 3.7 eV (Ref. 14) and 3.78 eV (Ref. 41), which is slightly smaller than 3.96 eV.[42] In addition, due to the GGA-PBE function usually underestimates the bandgaps for materials, the predicted bandgap for β-nitrogene is a little lower than that of the HSE06 function. For many results, the calculation energy gap (Eg) by the HSE method is larger than that of the DFT-PBE method with sufficiently reliable results.[14–19] Furthermore, the γ-nitrogene monolayer has a small energy gap (Eg) with semiconductor behavior, this result demonstrates that γ-nitrogene can be used for photoelectronic devices.

3.4. *Charge density*

The charge density of the β- and γ-nitrogene is described in Fig. 8. The arc triangle charge density distribution is encircled by the N atoms. As shown in Fig. 8, the cyan region indicates the increase in electron density after bonding. In summary, the large charge distributions in β- and γ-nitrogene are strong interactions between different N atoms, showing that the β- and γ-nitrogene have high system stability.

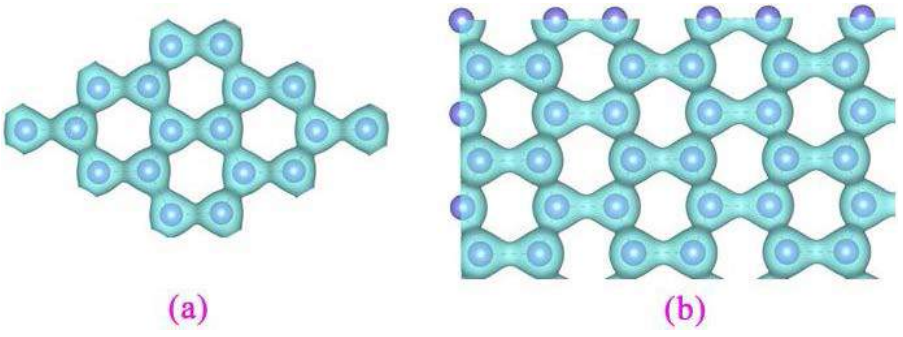

Fig. 8. (Color online) The charge density plots of (a) β-nitrogene and (b) γ-nitrogene.

3.5. *Optical properties*

Because the electronic structure of a material determines its optical properties, the electronic structure can be characterized by a dielectric function and a light absorption coefficient. The optical properties of the material include the real part $\varepsilon_1(\omega)$ and the imaginary part $\varepsilon_2(\omega)$ of the dielectric function, absorption $a(\omega)$, and refractive index $n(\omega)$, as previously reported.[43–47]

The imaginary part of the dielectric function is correlated with the real part of the dielectric function, and it can be obtained by using the Kramers–Kronig relation[48]:

$$\varepsilon(\omega) = \varepsilon_1(\omega) + i\varepsilon_2(\omega), \tag{4}$$

$$\varepsilon_2 = \frac{4\pi^2}{m^2\omega^2} \sum_{V,C} \int_{BZ} d^3k \frac{2}{(2\pi)} |e \cdot M_{cv}(K)|^2 \delta[E_C(k) - E_V(k) - h\omega], \tag{5}$$

$$\varepsilon_1 = 1 + \frac{8\pi^2 e^2}{m^2} \sum_{V,C} \int_{BZ} d^3k \frac{2}{(2\pi)} \frac{|e \cdot M_{CV}(K)|^2}{[E_C(k) - E_V(k)]} \frac{h^3}{[E_C(k) - E_V(k)]^2 - h^{-2}\omega^2}. \tag{6}$$

In Fig. 10, we show the absorption coefficient ($a(\omega)$) which can be written as[49]

$$\alpha(\omega) = \sqrt{2}[\sqrt{\varepsilon_1(\omega)^2 - \varepsilon_2(\omega)^2} - \varepsilon_1(\omega)]^{1/2}. \tag{7}$$

The real part and imaginary part $\varepsilon_1(\omega)$ as a function of β-nitrogene and γ-nitrogene are described in Fig 9. From Fig. 9(a), the calculated static dielectric constants (ε_0) of β- and γ-nitrogene are 1.17 and 1.21, respectively. The results show that the static dielectric constant of the γ-nitrogene is higher than that of the β-nitrogene. The value of the static dielectric constant also represents the ability to store electromagnetic fields. When the energy is greater than 17 eV, the tendency of the real part $\varepsilon_1(\omega)$ of the β-nitrogene spectrum is identical to that corresponding to the γ-nitrogene.

Figure 9(b) shows the imaginary part $\varepsilon_1(\omega)$ of the β- and γ-nitrogene. As seen from $\varepsilon_1(\omega)$, the absorption edges of β- and γ-nitrogene are 4.05 eV and 1.29 eV,

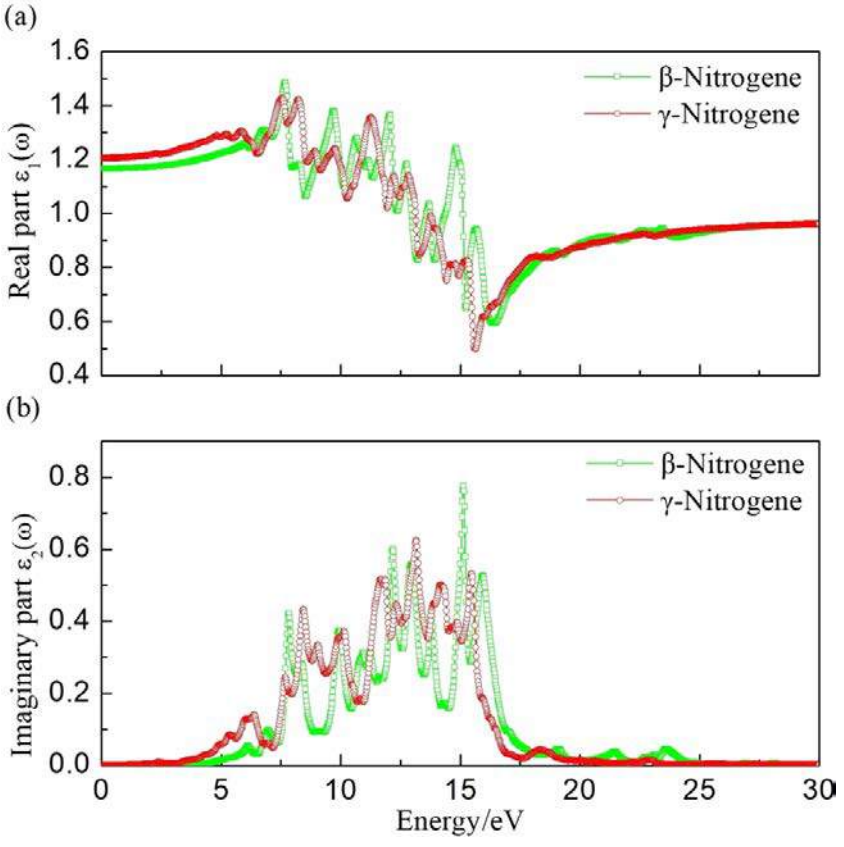

Fig. 9. (Color online) The real and imaginary parts for β-nitrogene and γ-nitrogene.

respectively. This is closely related to the energy gap (Eg), and the dielectric function is a microphysical process linking the band structure and spectral information. During this process, the electronic transitions between the energy levels produce spectra such that the dielectric peak can be explained by the band structures. It can be seen that the main dielectric peaks of the β-nitrogene are at 7.85, 9.89, 12.15, 12.96, 15.14, and 15.89 eV, and have a maximum value of 0.77 at 15.14 eV. In this case, the polarization current has the highest conductivity. In addition, from Fig. 9(b), it can also be seen that the main dielectric peaks of the γ-nitrogene are around 6.29, 8.47, 10.17, 11.67, 13.17, 14.26 and 15.41 eV, and it has a maximum value of 0.62 at 13.17 eV. When the photon energy is 0.50 eV–25.00 eV, the dielectric functions of β- and γ-nitrogene are $\varepsilon_2(\omega) > 0$. This shows that the β- and γ-nitrogene have a certain absorption of visible light and ultraviolet light. These results are consistent with the band structure calculations.

The absorption coefficient and refractive indices for both β- and γ-nitrogene are shown in Fig. 10. The absorption coefficient can describe the attenuation of

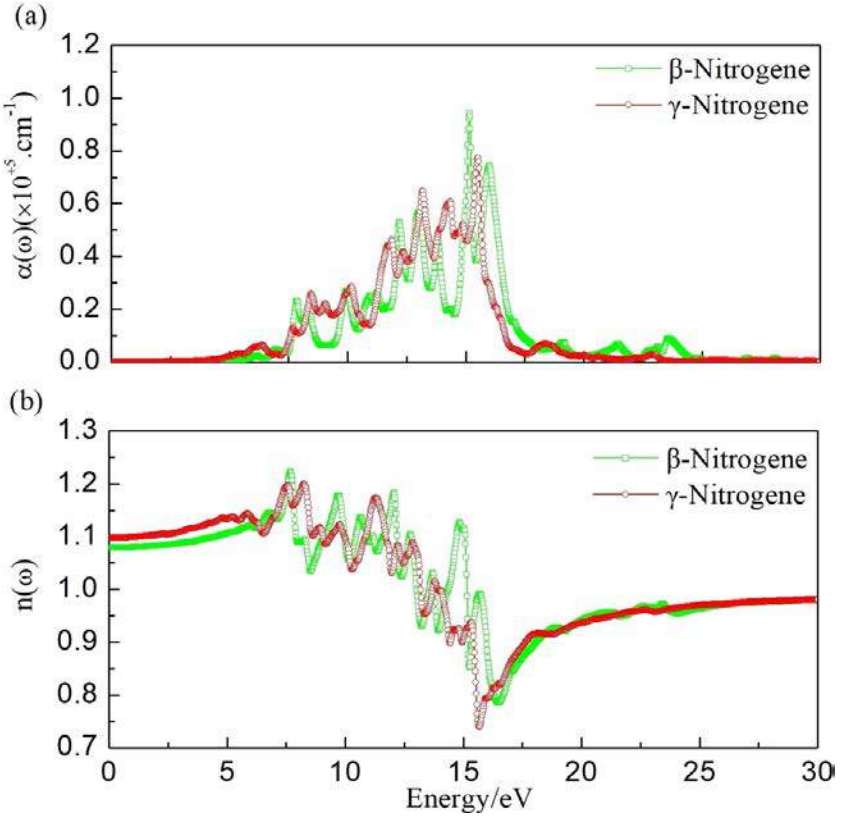

Fig. 10. (Color online) Absorption coefficient and refractive index of β-nitrogene and γ-nitrogene.

the light intensity per unit distance of light propagation in the medium. It reflects the change in the transitions produced by the increase in energy after the material absorbs photons. From Fig. 10(a), we can see that the absorption edges of β- and γ-nitrogene start from 4.05 and 1.29 eV, which corresponds to the imaginary part results. The two conditions originate from the excited electrons transition and N-p_z state located at the valence band maximum.

For β-nitrogene, when the photon energy reaches approximately 15.14 eV, the absorption peak reaches a maximum value of 0.93 and the energy width is from 4.05 eV∼25.00 eV. This result shows that β-nitrogene has a certain absorption effect on violet light and ultraviolet light. The absorption of violet light is weak, while the far-UV absorption is strong (6.20 eV–16.00 eV). For the γ-nitrogene, when the photon energy reaches approximately 15.55 eV, the absorption peak reaches a maximum value of 0.76 and the energy width is 1.90 eV–23.38 eV. This result shows that γ-nitrogene has a certain absorption effect on the visible spectrum and ultraviolet light. The absorption of visible light is weak, but the far-UV absorption is strong (6.2 eV∼16.43 eV). The refractive index as a function of photon energy

has been presented for two nitrogene allotropes in Fig. 10(b). The value of $n(\omega)$ represents the ratio of the radiant flux of the refracted light to the radiant flux of the incident light. In Fig. 10(b), it can be seen that the static refractive index $n(0)$ of β- and γ-nitrogene is 1.07 and 1.10, correspondingly.

4. Conclusions

In summary, we have used the density functional theory in the generalized gradient approximation to calculate the electronic structure and optical properties of the β-nitrogene and γ-nitrogene. The results are summarized as follows:

(1) Phonon dispersion suggests that β- and γ-nitrogene are stable.
(2) The thermal conductivity of β-nitrogene is almost isotropic, while that of the γ-nitrogene is anisotropic. At room temperature, the thermal conductivity of β-nitrogene is 960.17 $\mathrm{W/m \cdot K}$. But the thermal conductivities of γ-nitrogene are 12.34 $\mathrm{W/m \cdot K}$ and 18.59 $\mathrm{W/m \cdot K}$ along with the armchair and zigzag directions, respectively.
(3) β-nitrogene is an indirect bandgap semiconductor with a wide gap of 3.70 eV, and γ-nitrogene is also an indirect bandgap semiconductor with a narrow gap of 0.79 eV.
(4) The static refractive index of γ-nitrogene is larger than that of β-nitrogene.
(5) The γ-nitrogene has a certain absorption effect on the visible spectrum and ultraviolet light.

Thus, the different structure allotropes have different properties. Furthermore, the γ-nitrogene can be used to fabricate optoelectronic devices. This work provides theoretical guidance for the preparation of nitrogene allotropes photoelectric 2D devices.

Acknowledgments

This work was supported by the Key Research and Development Program of Shaanxi Province (No. 2020QFY-05-04), and Scientific Research Program Funded by Shaanxi Provincial Education Department (No. 20JS161). Z. Gao acknowledges the support of the National Natural Science Foundation of China (No. 12104356), China Postdoctoral Science Foundation (No. 2022M712552), and the Fundamental Research Funds for the Central Universities. We also acknowledge the support by the HPC Platform, Xi'an Jiaotong University.

References

1. V. O. Özcelik, O. Ü. Aktürk, E. Durgun and S. Ciraci, *Phys. Rev. B* **92** (2015) 125420.
2. E. S. Reich, *Nature* **506** (2014) 19.
3. C. Kamal and M. Ezawa, *Phys. Rev. B* **91** (2015) 085423.
4. O. Ü. Aktürk, V. O. Özçelik and S. Ciraci, *Phys. Rev. B* **91** (2015) 235446.

5. J. Ji, X. Song, J. Liu, Z. Yan, C. Huo, S. Zhang and Y. Hao, *Nat. Commun.* **7** (2016) 13352.
6. E. Aktürk, O. Ü. Aktürk and S. Ciraci, *Phys. Rev. B* **94** (2016) 014115.
7. F. F. Zhu, W. J. Chen, Y. Xu, C. L. Gao, D. D. Guan, C. H. Liu and J. F. Jia, *Nat. Mater.* **14** (2015) 1020.
8. Z. Zhu and D. Tománek, *Phys. Rev. Lett.* **112** (2014) 176802.
9. B. Wang, F. Guégan and G. Frapper, *J. Mater. Chem. C* **10** (2022) 10374.
10. P. Jureczko and M. Kurpas, *Sci. Rep.* **12** (2022) 3201.
11. H. Liu, A. T. Neal, Z. Zhu, Z. Luo, X. Xu, D. Tománek and P. D. Ye, *ACS Nano* **8**(4) (2014) 4033.
12. S. Zhang, Z. Yan, Y. Li, Z. Chen and H. Zeng, *Angew. Chem. Int. Ed* **127** (2015) 3155.
13. Y. Hu, T. Shu, C. Mao, L. Xue, Z. Yan and Y. Wu, *Physica B*: *Condens. Matter* **553** (2019) 195.
14. J. Lee, W. C. Tian, W. L. Wang and D. X. Yao, *Sci. Rep.* **5** (2015) 11512.
15. J. S. Li, W. L. Wang and D. X. Yao, *Sci. Rep.* **6** (2016) 34177.
16. Y. Zhang, J. Lee, W. L. Wang and D. X. Yao, *Comput. Mater. Sci.* **110** (2015) 109.
17. Y. Kadioglu, O. Üzengi Aktürk, E. Aktürk and S. Ciraci, *J. Phys. Chem. C* **121** (2017) 63298.
18. P. Li and W. Luo, *Sci. Rep.* **6** (2016) 25423.
19. B. Peng, D. Zhang, H. Zhang, H. Shao, G. Ni, Y. Zhu and H. Zhu, *Nanoscale* **9** (2017) 7397.
20. N. R. Glavin, R. Rao, V. Varshney, E. Bianco, A. Apte, A. Roy, E. Ringe, and P. M. Ajayan, *Adv. Mater.* **32** (2020) 1904302.
21. Z. Y. Ong, Y. Cai, G. Zhang and Y. W. Zhang, *J. Phys. Chem. C* **118** (2014) 25272.
22. G. Qin, Q. B. Yan, Z. Qin, S. Y. Yue, M. Hu and G Su, *Phys. Chem. Chem. Phys.* **17** (2015) 4854.
23. Z. Tian, S. Lee and G. Chen, *J. Heat Transf.* **135** (2013) 061605.
24. R. Fei, A. Faghaninia, R. Soklaski, J. Yan, C. Lo and L. Yang, *Nano Lett.* **14** (2014) 6393.
25. K. X. Chen, S. S. Lyu, X. M. Wang, Y. Fu, Y. Heng and D. C. Mo, *J. Phys. Chem. C* **121** (2017) 13035.
26. S. D. Wang, W. H. Wang and G. J. Zhao, *Phys. Chem. Chem. Phys.* **18** (2016) 31217.
27. J. Carrete, L. J. Gallego and N. Mingo, *J. Phys. Chem. Lett.* **8** (2017) 1375.
28. Y. Sun, D. Wang and Z. Shuai, *J. Phys. Chem. C* **121** (2017) 19080.
29. L. Cheng, H. Liu, X. Tan, J. Zhang, J. Wei, H. Lv, J. Shi and X. Tang, *J. Phys. Chem. C* **118** (2014) 904.
30. G. Kresse and J. Furthmüller, *Comput. Mater. Sci.* **6** (1996) 15.
31. G. Kresse and D. Joubert, *Phys. Rev. B* **59** (1999) 1758.
32. J. P. Perdew, K. Burke and M. Ernzerhof, *Phys. Rev. Lett.* **77** (1996) 3865.
33. Z. Cui, X. Wang, Y. Ding, E. Li, K. Bai, J. Zheng and T. Liu, *Appl. Surf. Sci.* **530** (2020) 147275.
34. Y. Ding, C. You, Y. Xu, L. Zhong, Q. Deng, J. Li and B. Xiao, *Appl. Surf. Sci.* **559** (2021) 149849.
35. Z. Cui, K. Bai, Y. Ding, X. Wang, E. Li and J. Zheng, *Physica E* **123** (2020) 114207.
36. A. Togo and I. Tanaka, *Scr. Mater.* **108** (2015) 1.
37. W. Li, N. Mingo, L. Lindsay, D. A. Broido, D. A. Stewart and N. A. Katcho, *Phys. Rev. B* **85** (2012) 195436.
38. W. Li, J. Carrete, N. A. Katcho and N. Mingo, *Comput. Phys. Commun.***185** (2014) 1747.
39. Y. Ding, B. Xiao, G. Tang and J. Hong, *J. Phys. Chem. C* **121** (2017) 225.

40. J. He, Y. Ouyang, C. Yu, P. Jiang, W. Ren and J. Chen, *Chin. Phys. B* **29** (2020) 126503.
41. R. Li and Y. Tao, *Nanotechnology* **31** (2020) 205202.
42. Y. Kadioglu, O. Üzengi Aktürk, E. Aktürk and S. Ciraci, *J. Phys. Chem. C* **121** (2017) 6329.
43. H. Lashgari, A. Boochani, A. Shekaari, S. Solaymani, E. Sartipi and R. T. Mendi, *Appl. Surf. Sci.* **369** (2016) 76.
44. M. Legesse, G. Fagas and M. Nolan, *Appl. Surf. Sci.* **396** (2016) 1155.
45. M. Shahrokhi and C. Leonard, *J. Alloy. Comp.* **693** (2017) 1185.
46. H. R. Mahida, A. Patel, D. Singh, Y. Sonvane, P. B. Thakor and R. Ahuja, *Superlattices Microstruct.* **162** (2022) 17132.
47. C. Cong, J. Shang, Y. Wang and T. Yu, *Adv. Opt. Mater.* **6** (2018) 1700767.
48. E. Shiles, T. Sasaki, M. Inokuti and D. Y. Smith, *Phys. Rev. B* **22** (1980) 1612.
49. A. Hashmi and J. Hong, *J. Magn. Magn. Mater.* **355** (2014) 7.